

Three-hadron angular correlations from pQCD at RHIC and LHC

Alejandro Ayala¹, Jamal Jalilian-Marian², Antonio Ortiz¹, Guy Paic¹, J. Magnin³ and Maria Elena Tejeda-Yeomans⁴

¹*Instituto de Ciencias Nucleares, Universidad Nacional Autónoma de México,
Apartado Postal 70-543, México Distrito Federal 04510, Mexico.*

²*Department of Natural Sciences, Baruch College, New York,
New York 10010, USA and CUNY Graduate Center,
365 Fifth Avenue, New York, New York 10016, USA.*

³*Centro Brasileiro de Pesquisas Físicas, CBPF, Rua Dr. Xavier Sigaud 150, 22290-180, Rio de Janeiro, Brazil.*

⁴*Departamento de Física, Universidad de Sonora, Boulevard Luis Encinas J. y Rosales,
Colonia Centro, Hermosillo, Sonora 83000, Mexico.*

We study three-hadron azimuthal angular correlations in high energy proton-proton and central nucleus-nucleus collisions at RHIC and LHC at mid-rapidity. We use the LO parton matrix elements for $2 \rightarrow 3$ processes and include the effect of parton energy loss in the Quark-Gluon Plasma using the modified fragmentation function approach. For the case when the produced hadrons have either same or not too different momenta, we observe two away side peaks at $2\pi/3$ and $4\pi/3$. We consider the dependence of the angular correlations on energy loss parameters that have been used in studies of single inclusive hadron production at RHIC. Our results on the angular dependence of the cross section agree well with preliminary data by the PHENIX collaboration. We comment on the possible contribution of $2 \rightarrow 3$ processes to di-hadron angular correlations and how a comparison of the two processes may help characterize the plasma further.

PACS numbers: 25.75.-q, 25.75.Gz, 12.38.Bx

I. INTRODUCTION

Jet quenching, the energy loss of a parton moving in a Quark-Gluon Plasma (QGP), is one of the key paradigms emerging from high energy heavy ion collisions at the Relativistic Heavy Ion Collider (RHIC) and the Large Hadron Collider (LHC). This energy loss is believed to cause the suppression of single hadron transverse momentum spectra in Au + Au collisions, as compared to p + p collisions, as well as the disappearance of the away-side peak in two-particle azimuthal correlations [1]. Nevertheless, the fact that many different energy loss models can fit the observed suppression of single and double inclusive hadrons, produced in high energy heavy ion collisions, makes it imperative to consider more exclusive observables in order to shed light on the dynamics of energy loss. One can ask for example whether the *double hump* structure on the away-side in azimuthal two-particle correlations in Au + Au collisions [2] can be studied from looking at more exclusive channels such as three-hadron correlations. These studies have shown to provide a powerful tool to distinguish between different proposed scenarios [3, 4].

This question has been addressed in Ref. [5] where we showed that some properties of the two-particle correlations can be understood from three-hadron production studies. The connection is made by considering the different path lengths traveled by the two away side partons in $2 \rightarrow 3$ versus the away side parton in $2 \rightarrow 2$ parton processes. In the former, one of the two final state partons in the away side travels, on the average, a larger path length than the other and also larger than the away side parton in the latter processes, leading to an increase in the probability of absorption of this parton due to en-

ergy loss. Since the parton that travels the smaller path length in $2 \rightarrow 3$ processes in the away side has on the average, also a smaller path length to go through than the away side parton in $2 \rightarrow 2$ processes, the parton in the former has a smaller chance of losing energy than its counterpart in the latter processes. The combination of these two effects effectively amplifies the production of structures that upon accumulation of signal look like a double hump or a broader peak in the away side, depending on the momentum difference between leading and associate particles.

To look closer at this issue, in this work we consider the three-hadron production cross sections in p + p and A + A collisions using leading order (LO) $2 \rightarrow 3$ partonic processes. To include the effect of QGP and parton energy loss on the final particle spectra, we use modified fragmentation functions. We then investigate the effect of energy loss on the angular correlations of the three produced hadrons by varying the parameters associated with the energy loss suffered by each parton. We compare our results to the preliminary data on three-hadron correlation function measured at RHIC and find that the angular dependence of the correlation function is reproduced correctly by our formalism.

The work is organized as follows: in Sec. II we write the three-hadron production cross section in p + p and also introduce the modified fragmentation function which takes parton energy loss into account for A + A collisions. We show the time-evolved profile of the medium and the average number of scatterings as functions of the initial points and trajectories on the transverse plane for central collisions. In Sec. III we investigate the dependence of the three-hadron production cross section at RHIC and LHC on energy loss parameters. We then compare our

results to preliminary data on the angular correlations of the three produced hadrons and show that there is a good agreement in the kinematic range accessible by our formalism. We conclude in Sec. IV by pointing out to the possible contributions of $2 \rightarrow 3$ processes to di-hadron correlations and how they may probe different transverse plane evolution of the hard scatterings within the plasma.

II. THREE-HADRON PRODUCTION

The differential cross section for three-hadron production, with momenta h_1 , h_2 , h_3 , in $p + p$ collisions in mid-rapidity is given by

$$\left(\frac{d\sigma}{d\theta_2^H d\theta_3^H dh_1 dh_2 dh_3} \right)^{pp \rightarrow H_1 H_2 H_3} = \frac{1}{h_1 h_2 h_3} \sum_{i,j} \frac{1}{3!} \sum_{\substack{\text{permutations} \\ k \neq l \neq m}} \frac{F(\theta_2, \theta_3)}{8(2\pi)^4} \int_0^1 dx_1 x_1 f_{i/p}(x_1) x_1 f_{j/p}(x_1) D_{P_k/H_1}(z_{1k}) D_{P_l/H_2}(z_{2l}) D_{P_m/H_3}(z_{3m}) |\mathcal{M}_{ij \rightarrow P_k P_l P_m}|^2 \quad (1)$$

where $f_{i/p}$ and $f_{j/p}$ are the distribution functions of partons i, j within the colliding protons. We use the CTEQ6 parametrization [6]. $\mathcal{M}_{ij \rightarrow P_k P_l P_m}$ is the corresponding leading order matrix element describing the process at the parton level [7].

The sum is over all the possible colliding parton species, over all of the three possible partons in the final state and over all the permutations for a given parton in the final state to become a given hadron. The magnitudes of the final state parton momenta are determined from momentum conservation at the parton level as functions of the angles that \vec{p}_2 and \vec{p}_3 (θ_2 , θ_3 , respectively) make with \vec{p}_1

$$\begin{aligned} p_1 &= \frac{x_1 \sqrt{s} \sin(\theta_3 - \theta_2)}{\sin(\theta_3 - \theta_2) + \sin \theta_2 - \sin \theta_3} \\ p_2 &= \frac{-x_1 \sqrt{s} \sin \theta_3}{\sin(\theta_3 - \theta_2) + \sin \theta_2 - \sin \theta_3} \\ p_3 &= \frac{x_1 \sqrt{s} \sin \theta_2}{\sin(\theta_3 - \theta_2) + \sin \theta_2 - \sin \theta_3}, \end{aligned} \quad (2)$$

where \sqrt{s} is the total center of mass energy available for the collision. x_1 is the momentum fraction of the incoming parton in the projectile. The momentum fraction of the incoming parton in the target is fixed also by momentum conservation to be x_1 . The angular dependent part of the phase space factor is

$$F(\theta_2, \theta_3) = \frac{-\sin \theta_3 \sin \theta_2 \sin(\theta_3 - \theta_2)}{[\sin(\theta_3 - \theta_2) + \sin \theta_2 - \sin \theta_3]^4} \quad (3)$$

and $D_{P_n/H_m}(h_m/p_n)$, is the fragmentation function of parton P_n to become hadron H_m , which is a function of the momentum fraction $z_{nm} = h_m/p_n$ ($n, m = 1, 2, 3$). We take the fragmentation functions for charged hadrons as given by the KKP parametrization [8]. In each permutation, any given parton can become the leading hadron which, we take as H_1 , and the other two the away-side hadrons. We work in the limit of collinear fragmentation thus, the angles that define the direction of the away-side hadrons, θ_i^H ($i = 2, 3$), are linearly related to the the parton angles θ_j ($j = 2, 3$).

To consider the process within a central heavy-ion collision and thus account for the effects of energy loss, we resort to the model put forward in Ref. [9]. The model considers an initial gluon density obtained from the overlap of two colliding nuclei, each with a Woods-Saxon density profile. The gluon density of the medium is diluted only due to longitudinal expansion of the plasma since transverse expansion is neglected.

The gluon density ρ_g is related to the nuclear geometry of the produced medium as

$$\begin{aligned} \rho_g(\tau, \vec{b}, \vec{r}, \hat{n}) &= \frac{\tau_0 \rho_0}{\tau} \frac{\pi R_A^2}{2A} \\ &\times \left[T_A(|\vec{r} + \hat{n}\tau|) + T_A(|\vec{b} - \vec{r} - \hat{n}\tau|) \right], \end{aligned} \quad (4)$$

where T_A is the nuclear thickness function, R_A is the nuclear radius and A the atomic number.

We use the modified fragmentation functions

$$\tilde{D}_{P_n/H_m}(z_{nm}) = \left(1 - e^{-(L/\lambda)} \right) \left[\frac{z'_{nm}}{z_{nm}} D_{P_n/H_m}(z'_{nm}) + \langle L/\lambda \rangle \frac{z'_{nm;g}}{z_{nm}} D_{P_n/H_m}(z'_{nm;g}) \right] + e^{-(L/\lambda)} D_{P_n/H_m}(z'_{nm}), \quad (5)$$

where $z'_{nm} = h_m/(p_n - \Delta E_n)$ is the rescaled momentum fraction, of hadron H_m originated from the fragmenting parton P_n , $z'_{nm;g} = \langle L/\lambda \rangle (h_m/\Delta E_n)$ is the rescaled mo-

mentum fraction of the radiated gluon, ΔE_n is the average radiative parton energy loss and $\langle L/\lambda \rangle$ is the average number of scatterings. The energy loss ΔE_n is related to

the gluon density of the produced medium via

$$\Delta E_n = \left\langle \frac{dE_n}{dL} \right\rangle_{1d} t(r, \varphi) \quad (6)$$

where

$$t(r, \varphi) \equiv \int_{\tau_0}^{\infty} d\tau \frac{\tau - \tau_0}{\tau_0 \rho_0} \rho_g(\tau, \vec{b}, \vec{r}, \hat{n}) \quad (7)$$

and \vec{b} is the impact parameter of the collision, \vec{r} is the transverse plane location of the hard scattering where the partons are produced and \hat{n} is the direction in which the produced hard parton travels in the medium. r and φ are the radial position and the angle that \hat{n} makes with the radial direction, respectively. The function $t(r, \varphi)$ can be interpreted as the *medium influence time*, that is the time during which the medium makes a parton lose energy, when it was produced at r and starts traveling through the medium making an angle φ with the radial direction. The parameter τ_0 is the formation time for the medium gluons and ρ_0 is the initial central gluon density. τ is the time elapsed from the formation time and parametrizes the path length over the trajectory of the parton within the plasma. Since the gluon density profile is a rapidly falling function, the upper limit of integration can be safely set to infinity. Figure 1 shows $t(r, \varphi)$ for a central collision. Notice that because of the dilution of the medium due to longitudinal expansion of the plasma, the biggest effect is on partons which have to travel less than the full length of the plasma, i.e. partons

which are produced around two thirds from the center of plasma on the transverse plane.

The average number of scatterings for a given parton is

$$\left\langle \frac{L}{\lambda} \right\rangle = \int_{\tau_0}^{\infty} d\tau \frac{1}{\lambda_0 \rho_0} \rho_g(\tau, \vec{b}, \vec{r}, \hat{n}), \quad (8)$$

where λ_0 is the parton mean free path. Since we want to consider the most central collisions, hereafter we set $\vec{b} = 0$. The one dimensional energy loss $\langle dE_n/dL \rangle_{1d}$ is parameterized as

$$\left\langle \frac{dE_n}{dL} \right\rangle_{1d} = \epsilon_0 \left[\frac{p_n}{\mu_0} - 1.6 \right]^{1.2} \left[7.5 + \frac{p_n}{\mu_0} \right]^{-1}. \quad (9)$$

The one-dimensional energy loss per unit length parameter, ϵ_0 , is related to the mean free path λ_0 by $\epsilon_0 \lambda_0 = 0.5$ GeV. We work with a value $\mu_0 = 1.5$ GeV and refer the reader to Refs. [9–12] for explicit details of the meaning and values of the introduced parameters.

Figure 2 shows the average number of scatterings per unit length for a central collision. Shown is the case for $\epsilon_0 = 1.5$ GeV/fm for which the maximum average number of collisions is about 2.5. The average number of collisions grows with ϵ_0 . As is clear from the figure, particles that experience the largest average number of collisions are the ones that are produced around one third from the center and travel opposite to the radial direction, toward

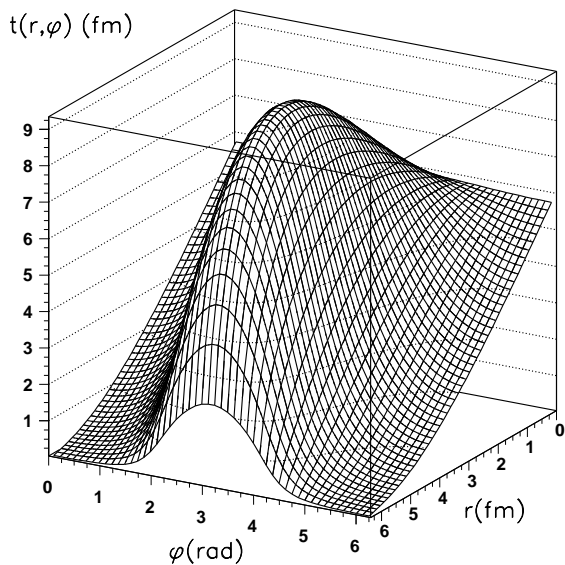


FIG. 1: Medium influence time $t(r, \varphi)$ for a central collision as a function of all the initial points and trajectories on the transverse plane for a central collision. The initial points are characterized by their radial position r and the angle that the parton trajectory makes with the outward radial direction φ .

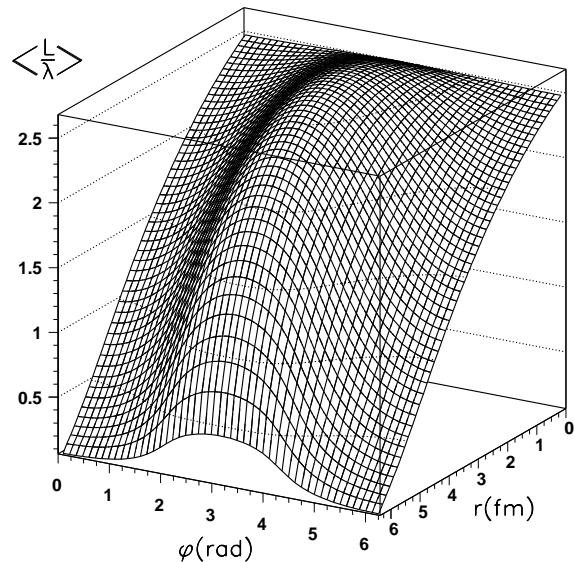


FIG. 2: Average number of scatterings as a function of all the initial points and trajectories on the transverse plane for a central collision. The initial points are characterized by their radial position r and the angle that the parton trajectory makes with the outward radial direction φ . Shown is the case for $\epsilon_0 = 1.5$ GeV/fm.

the interior of the medium. This effect can also be understood as arising from the dilution of the medium due to longitudinal expansion of the plasma.

Given the above, the differential cross section for production of three hadrons with momenta h_1 , h_2 , h_3 at mid-rapidity in A + A collisions is given by

$$\begin{aligned}
 \left(\frac{d\sigma}{d\theta_2^H d\theta_3^H dh_1 dh_2 dh_3} \right)^{AA \rightarrow H_1 H_2 H_3} &= \int \frac{d^2 r}{\pi R_A^2} \frac{d\varphi}{2\pi} \left(\frac{d\tilde{\sigma}}{d\theta_2^H d\theta_3^H dh_1 dh_2 dh_3} \right)^{pp \rightarrow H_1 H_2 H_3}, \\
 &= \frac{1}{h_1 h_2 h_3} \sum_{i,j} \frac{1}{3!} \sum_{\substack{\text{permutations} \\ k \neq l \neq m}} \frac{F(\theta_2, \theta_3)}{8(2\pi)^4} \int \frac{d^2 r}{\pi R_A^2} \frac{d\varphi}{2\pi} \int_0^1 dx_1 x_1 f_{i/p}(x_1) x_1 f_{j/p}(x_1) \\
 &\times \tilde{D}_{P_k/H_1}(z_{1k}) \tilde{D}_{P_l/H_2}(z_{2l}) \tilde{D}_{P_m/H_3}(z_{3m}) |\mathcal{M}_{ij \rightarrow P_k P_l P_m}|^2,
 \end{aligned} \tag{10}$$

where the new integrations with respect to the p + p case are performed over the overlap area of the nuclear collision and over the angle φ that the direction of emission of the leading hadron makes with respect to the radial direction. We have correspondingly divided by the nuclear overlap area πR_A^2 and by 2π in order to have the per nucleon yield.

The matrix elements $\mathcal{M}_{ij \rightarrow P_k P_l P_m}$ in Eqs. (1) and (10), representing the $2 \rightarrow 3$ LO QCD hard scattering amplitudes at the parton level are divergent due both to collinear and soft singularities. These kinematic divergences are universal and can be removed using well known techniques [13, 14]. Here instead we apply angu-

lar cuts to avoid the divergent regions. An alternative is to use an automated version of the dipole subtraction method [15] in the MadGraph environment [16]. This avenue is being explored and will be reported elsewhere. Hereafter, $\mathcal{M}_{ij \rightarrow P_k P_l P_m}$ stands for the finite matrix elements, after applying angular cuts. Throughout we use the factorization and renormalization scales μ_f and μ_r as $\mu_r = \mu_f = 2$ GeV.

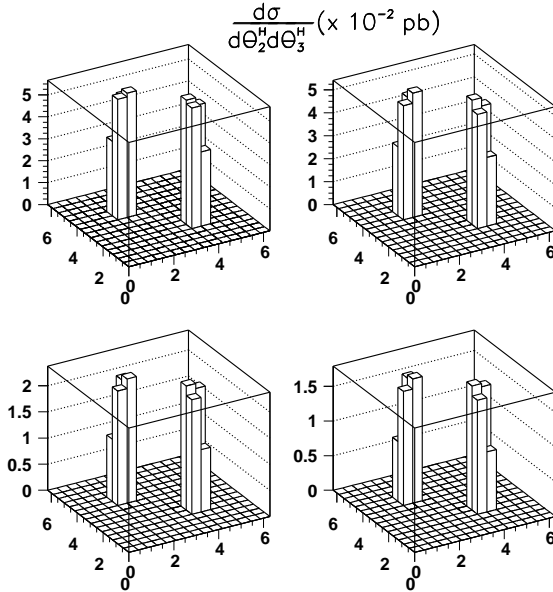


FIG. 3: Cross section ($d\sigma/d\theta_2^H d\theta_3^H$) for a symmetric hadron momentum configuration where $2 \text{ GeV} \leq h_1, h_2, h_3 \leq 3 \text{ GeV}$ with $\sqrt{s_{NN}} = 200 \text{ GeV}$. From left to right and top to bottom are the p + p case and the A + A cases for $\epsilon_0 = 0.1, 1.5, 2 \text{ GeV/fm}$, respectively.

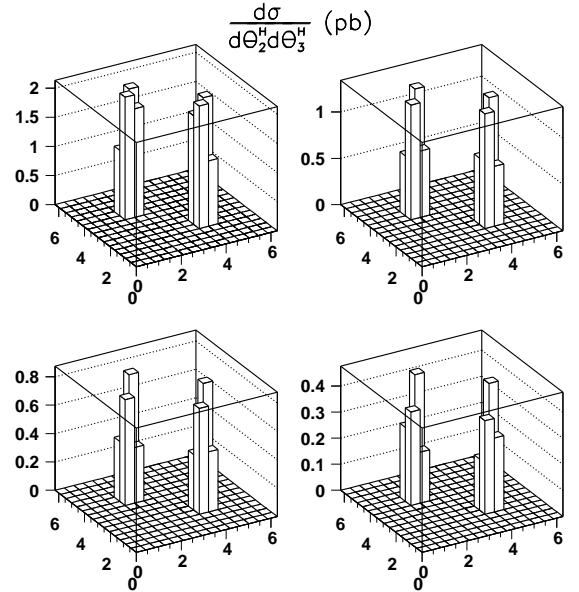


FIG. 4: Cross section ($d\sigma/d\theta_2^H d\theta_3^H$) for a symmetric hadron momentum configuration where $2 \text{ GeV} \leq h_1, h_2, h_3 \leq 3 \text{ GeV}$ with $\sqrt{s_{NN}} = 2.76 \text{ TeV}$. From left to right and top to bottom are the p + p case and the A + A cases for $\epsilon_0 = 2, 3, 4 \text{ GeV/fm}$, respectively.

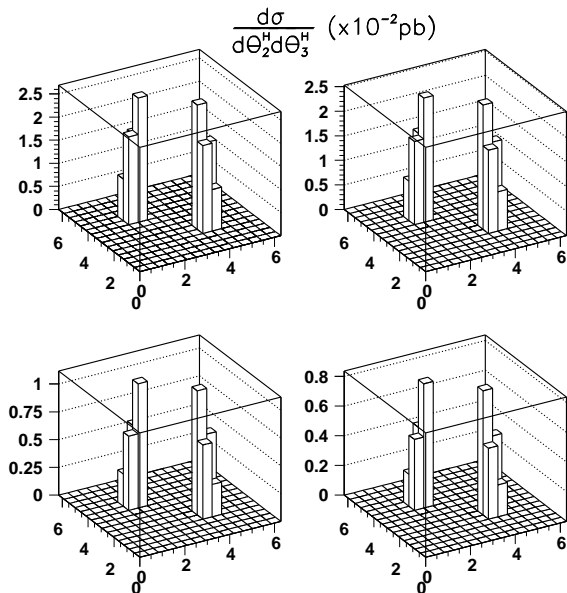


FIG. 5: Cross section ($d\sigma/d\theta_2^H d\theta_3^H$) for an asymmetric hadron momentum configuration where $3 \text{ GeV} \leq h_1 \leq 4 \text{ GeV}$ and $2 \text{ GeV} \leq h_2, h_3 \leq 3 \text{ GeV}$ with $\sqrt{s_{NN}} = 200 \text{ GeV}$. From left to right and top to bottom are the p + p case and the A + A cases for $\epsilon_0 = 0.1, 1.5, 2 \text{ GeV/fm}$, respectively.

III. THREE-HADRON CORRELATIONS

Figure 3 shows the contribution of $2 \rightarrow 3$ processes to the three-hadron correlation function. Shown is the cross section ($d\sigma/d\theta_2^H d\theta_3^H$) for a symmetric hadron momentum configuration where $2 \text{ GeV} \leq h_1, h_2, h_3 \leq 3 \text{ GeV}$ with a collision energy of $\sqrt{s_{NN}} = 200 \text{ GeV}$, appropriate for RHIC energies. From left to right and top to bottom, the figure shows the p + p case and the A + A cases for values of the one-dimensional energy loss per unit length parameter $\epsilon_0 = 0.1, 1.5, 2 \text{ GeV/fm}$, respectively. These values are chosen to correspond to the ones explored in Ref. [9]. In these plots $\pi/5 \leq \theta_2^H (\theta_3^H) \leq 4\pi/5, 6\pi/5 \leq \theta_3^H (\theta_2^H) \leq 9\pi/5$. The excluded region corresponds, to events with only two hadrons in the final state, within our resolution. We also notice that when $\epsilon_0 \rightarrow 0$, the correlation function in the p + p case is recovered and that with increasing values of ϵ_0 the intensity of the signal decreases, as expected.

Figure 4 shows also the contribution of $2 \rightarrow 3$ processes to the three-hadron correlation function for a symmetric hadron momentum configuration $2 \text{ GeV} \leq h_1, h_2, h_3 \leq 3 \text{ GeV}$ but this time for a collision energy of $\sqrt{s_{NN}} = 2.76 \text{ TeV}$, appropriate for LHC energies. From left to right and top to bottom, the figure shows the p + p case and the A + A cases for values of the one-dimensional energy loss per unit length parameter $\epsilon_0 = 2, 3, 4 \text{ GeV/fm}$, respectively. As in Fig. 3 for these plots $\pi/5 \leq \theta_2^H (\theta_3^H) \leq 4\pi/5, 6\pi/5 \leq \theta_3^H (\theta_2^H) \leq 9\pi/5$. We also notice from Fig. 4

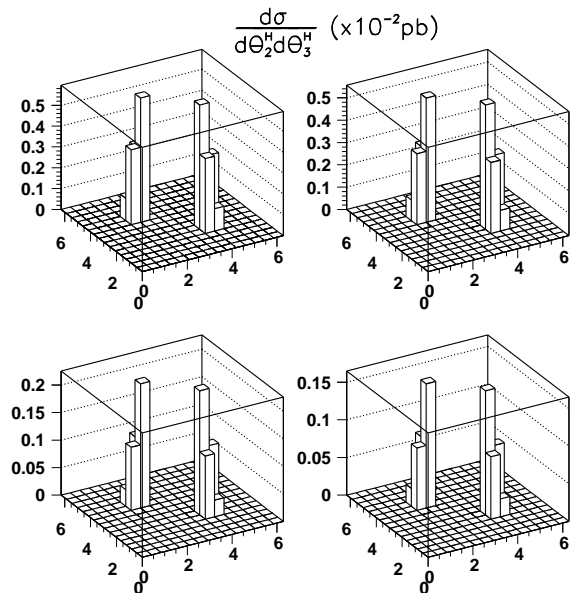


FIG. 6: Cross section ($d\sigma/d\theta_2^H d\theta_3^H$) for an asymmetric hadron momentum configuration where $5 \text{ GeV} \leq h_1 \leq 6 \text{ GeV}$ and $2 \text{ GeV} \leq h_2, h_3 \leq 3 \text{ GeV}$ with $\sqrt{s_{NN}} = 200 \text{ GeV}$. From left to right and top to bottom are the p + p case and the A + A cases for $\epsilon_0 = 0.1, 1.5, 2 \text{ GeV/fm}$, respectively.

that with increasing values of ϵ_0 the intensity of the signal decreases, as expected.

Figures 5 and 6 show asymmetric hadron momenta configurations. Figure 5 shows the case where $3 \text{ GeV} \leq h_1 \leq 4 \text{ GeV}$ and $2 \text{ GeV} \leq h_2, h_3 \leq 3 \text{ GeV}$, whereas Fig. 6 is the case where $5 \text{ GeV} \leq h_1 \leq 6 \text{ GeV}$ and $2 \text{ GeV} \leq h_2, h_3 \leq 3 \text{ GeV}$, both calculated with $\sqrt{s_{NN}} = 200 \text{ GeV}$. Notice that the position of the two peaks on the away side remain at roughly $2\pi/3$ and $4\pi/3$ rad, as was the case for the symmetric configurations. Their intensity decreases with respect to the symmetric, lower momentum case of Fig. 3, as the difference between away and leading particle momenta increases but the higher value becomes sharper. Also, the intensity decreases as the energy loss parameter increases.

In order to extract information from the three-hadron correlation function in a two dimensional analysis, one possibility is to look at this object as a function of the angular difference $\Delta\phi = \theta_3^H - \theta_2^H$ of the away side particles for a range of angles of one of the away side-particles, say $\Delta\theta = \theta_2^H$. Figure 7 shows this correlation in a A + A environment with $\sqrt{s_{NN}} = 200 \text{ GeV}$ for a leading hadron momentum $2.5 \text{ GeV} \leq h_1 \leq 4 \text{ GeV}$ and away-side hadron momenta $1 \text{ GeV} \leq h_2, h_3 \leq 2.5 \text{ GeV}$, integrated over a θ_2^H angular range $1.65 \leq \Delta\theta \leq 2.2 \text{ rad}$. Shown are the histograms obtained for $\epsilon_0 = 1, 2, 3 \text{ GeV/fm}$ normalized to their cross section, σ , obtained by integration of the differential cross section over the above angular ranges and compared to preliminary data from PHENIX [4]. Due to our angular cuts, meant to exclude collinear hadron pro-

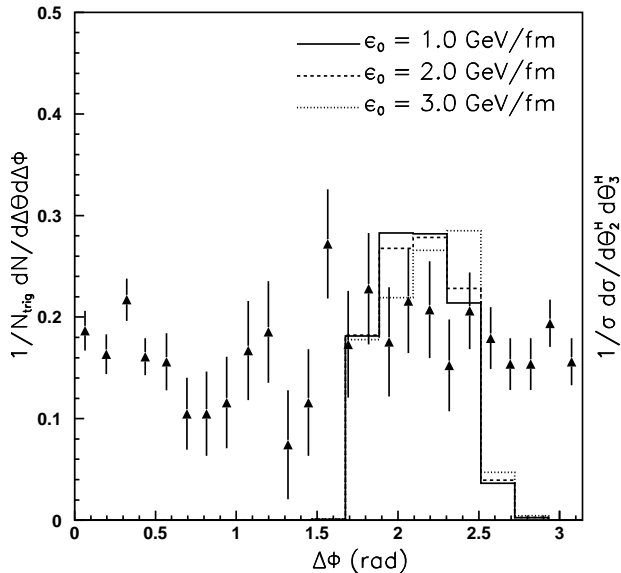


FIG. 7: Cross section $d\sigma/d\theta_2^H\theta_3^H$ as a function of the angular difference $\Delta\phi = \theta_3^H - \theta_2^H$ for a leading hadron momentum $2.5 \text{ GeV} \leq h_1 \leq 4 \text{ GeV}$ and away-side hadron momenta $1 \text{ GeV} \leq h_2, h_3 \leq 2.5 \text{ GeV}$ integrated over a $\Delta\theta = \theta_2^H$ angular range $1.65 \leq \Delta\theta \leq 2.2 \text{ rad}$. The histograms are normalized to their cross section, σ , obtained by integration of the differential cross section over the above angular ranges and correspond to three values of the energy loss parameter $\epsilon_0 = 1, 2, 3 \text{ GeV/fm}$. The calculation is compared to preliminary data from PHENIX.

duction, the regions $\Delta\phi \simeq 0, \pi \text{ rad}$ are not accessible. However, as is clear from the figure, the angular region $1.5 \lesssim \Delta\phi \lesssim 2.7 \text{ rad}$ is well described, particularly for the value of $\epsilon_0 = 2 \text{ GeV/fm}$.

IV. CONCLUSION

In this work we have calculated the three-hadron production cross sections in both $p + p$ and $A + A$ collisions and investigated the effect of parton energy loss on the angular correlations between the produced hadrons. We have considered collision energies appropriate for RHIC and LHC. For the cases where the hadrons have same or not too different momenta, studied in this work, we observe two peaks on the away side, with respect to the leading hadron, at roughly $2\pi/3$ and $4\pi/3 \text{ rad}$. The lo-

cation of the peaks stays the same and their intensity decreases as the difference between away and leading particle momenta increases. The intensity also drops as we increase the energy loss parameter.

There are a few interesting questions that warrant further work, for instance, one could consider the contribution of these $2 \rightarrow 3$ processes to di-hadron correlations. This could happen when either one of the partons travels a large distance in the plasma and loses a large portion of its energy, so that its transverse momentum is outside the transverse momentum window considered for the associate hadrons. Another possibility comes from the projection of the three-hadron angular correlation onto two-dimensions, i.e., when one integrates over one of the away side hadrons' angle.

It would be interesting to compare these contributions with those of genuine $2 \rightarrow 2$ processes. Naively, one might expect that for the case when there are three hadrons in the final state, the partonic hard scattering must happen close to the center of the plasma in the transverse plane. On the other hand, one expects that contributions of $2 \rightarrow 3$ processes to di-hadron correlations come from events where the partonic hard scattering happens closer to the edge, so that at least one of the partons travels a large distance through the medium and has a high probability of being completely absorbed. A study of the transverse plane location dependence of these events may thus provide more information for the tomography of the Quark-Gluon Plasma than is possible with single or even genuine double inclusive hadron production. This work is in progress and will be reported elsewhere.

Acknowledgments

A.A., J.J.-M. and M.E.T.-Y. thank CBPF for their kind hospitality and support during a visit where this work was completed. Support for this work has been received in part by CONACyT (Mexico) under grant number 128534, PAPIIT-UNAM under grant number IN103811-3, *Programa de Intercambio UNAM-UNISON*, the DOE Office of Nuclear Physics through Grant No. DE-FG02-09ER41620, by the "Lab Directed Research and Development" grant LDRD 10-043 (Brookhaven National Laboratory), and by The City University of New York through the PSC-CUNY Research Award Program, grant 63404-0041.

[1] S.S. Adler *et al.* (PHENIX Collaboration), Phys. Rev. Lett. **91**, 072301 (2003); J. Admas *et al.* (STAR Collaboration), Phys. Rev. Lett. **91**, 172302 (2003); S.S. Adler *et al.* (PHENIX Collaboration), Phys. Rev. C **69**, 034910 (2004); C. Adler *et al.* (STAR Collaboration), Phys. Rev.

Lett. **90** 082302 (2003); J. Adams *et al.* (STAR Collaboration), Nucl. Phys. A **757**, 102 (2005); J. Adams *et al.* (STAR Collaboration), Phys. Rev. Lett. **97**, 162301 (2006)

[2] J. Adams *et al.* (STAR Collaboration), Phys. Rev. Lett.

- 95**, 152301 (2005); A. Adare *et al.* (PHENIX Collaboration), Phys. Rev. C **77**, 011901(R) (2008); A. Adare *et al.* (PHENIX Collaboration), Phys. Rev. C **78**, 014901 (2008).
- [3] B.I. Abelev *et al.* (STAR Collaboration), Phys. Rev. Lett. **102**, 052302 (2009).
- [4] N.N. Ajitanand (for the PHENIX Collaboration), Indian J. Phys. **84**, 1647 (2010).
- [5] A. Ayala, J. Jalilian-Marian, J. Magnin, A. Ortiz, G. Paic and M. E. Tejada-Yeomans, Phys. Rev. Lett. **104**, 042301 (2010).
- [6] H. L. Lai, J. Huston, Z. Li, P. Nadolsky, J. Pumplin, D. Stump and C.P. Yuan, Phys. Rev. D **82**, 054021 (2010).
- [7] R.K. Ellis and J.C. Sexton, Nucl. Phys. B **269**, 445 (1986).
- [8] B.A. Kniehl, G. Kreimer and B. Potter, Nucl. Phys. B **582**, 514 (2000).
- [9] H. Zhang, J.F. Owens, E. Wang and X.-N. Wang, Phys. Rev. Lett. **98**, 212301 (2007).
- [10] M. Gyulassy, I. Vitev and X.-N. Wang, Phys. Rev. Lett. **86**, 2537 (2001)
- [11] E. Wang and X.-N. Wang, Phys. Rev. Lett. **87**, 142301 (2001); **89**, 162301 (2002).
- [12] C.A. Salgado and U. A. Wiedemann, Phys. Rev. Lett. **89**, 092303 (2002).
- [13] S. Catani and M.H. Seymour, Nucl. Phys. B **485**, 291 (1997).
- [14] Z. Kunszt and D.E. Soper, Phys. Rev. D **46**, 192 (1992).
- [15] R. Frederix, T. Gehrmann and N. Greiner, JHEP **0809**, 122 (2008); JHEP **1006**, 86 (2010).
- [16] J. Alwall *et al.*, JHEP **0709**, 28 (2007).